J|A|C|S
ARTICLES
Published on Web 09/21/2004

Electron-Deficient Bonding in ♦ Rhomboid Rings

Musiri M. Balakrishnarajan and Roald Hoffmann*

Contribution from the Department of Chemistry and Chemical Biology, Baker Laboratory, Cornell University, Ithaca, New York 14853

Received June 2, 2004; E-mail: rh34@cornell.edu

Abstract: The bonding environment of boron is usually thought about in terms of localized 2c−2e/3c−2e bonding (as in diborane) or completely delocalized polyhedral bonding (as in $B_{12}H_{12}^{2-}$). Recently, a number of boron compounds having a rhomboidal B_4 framework have been synthesized; these show an amazing variation in their skeletal electron count, one that cannot be interpreted in familiar ways. In this report, we systematically explore the origin of the range of electron counts in these compounds. We find that four skeletal MOs are primarily responsible for keeping the B_4 skeleton together. As a subunit in a macropolyhedral environment, termed *rhombo*-B_4, such an arrangement of B atoms deviates from Wade's rule by three electron pairs (if treated as a distorted *arachno* system derived from $B_6H_6^{2-}$). Aided by this analysis, we examine the nature of bonding in Na_3B_{20}, where the *rhombo*-B_4 unit forms linear chains fusing *closo*-B_7 units. Theory suggests that this structure requires one more electron per formula unit for optimal bonding. Finally, we study the nature of bonding in β-SiB_3, where silicon atoms also adopt the rhomboid framework.

Molecules with the geometry of a perfect square are rare for the main group elements. The exceptions are S_4^{2+}, Te_4^{2+}, Se_4^{2+}, and P_4^{2-} ions[1] and some organic systems with exocyclic double bonds.[2] A ring-puckering distortion of the square is common in saturated hydrocarbons such as cyclobutane and even in organic systems that should be aromatic by Hückel's rule.[3] Recently, a variety of electron-deficient, boron-containing molecules with characteristic, nearly planar rhombic rings[4−6] were synthesized. These systems appear to exist with a wide range of electron counts. The rhomboid is also found as a substructure in the recently characterized extended structures of Na_3B_{20}[7] and β-SiB_3.[8] In this report, we explore the nature of bonding in these systems, probing the mystery behind the persistence of the rhomboid skeleton in such diverse environments.

Figure 1 shows some representative examples of experimentally characterized molecules with a B_4 rhomboid skeleton. Assuming 2c−2e (two-centered-two electron) *exo*-rhomboid bonds, molecule **1a**[4a] has four electron pairs left for the bonding in the rhombus. Some related systems with a variety of substituents were also been reported.[4b,c] A similar assumption leads to three electron pairs for **1b**[5] and two electron pairs for **1c**.[6] Molecule **1d**, $B_{20}H_{18}^{2-}$, was synthesized 40 years ago;[9a] several polyhedra contain this rhomboid B_4 skeleton.[9] An interesting paradox in electron counting arises for $B_{20}H_{18}^{2-}$; it can be formally constructed from two $B_{10}H_{10}^{2-}$ molecules by removing two hydride ions. If we then allocate $(n + 1)$ electron pairs, $n = 10$, for the individual *closo*-B_{10} units, following Wade's rules,[10] we are left with the absurdity of having no electrons left to hold the two polyhedra together. It is clear that electrons in this system are delocalized over the entire skeleton. This rhomboidal framework is also observed in molecules where one or more boron atoms are replaced by isolobal transition-metal fragments.[11]

(1) (a) Brown, I. D.; Crump, D. B. J. *Inorg. Chem.* **1971**, *10*, 2319−2323. (b) Couch, T. W.; Lokken, D. A.; Corbett, J. D. *Inorg. Chem.* **1972**, *11*, 357−362. (c) Passmore, J.; Sutherland, G. White, P. S. *J. Chem. Soc., Chem. Commun.* **1980**, 330−331. (d) Passmore, J.; Sutherland, G. White, P. S. *Inorg. Chem*. **1982**, *21*, 2717−2723. (e) Nenajdenko, V. G.; Shevchenko, N. E.; Balenkova, E. S.; Alabugin, I. V. *Chem. Rev.* **2003**, *103*, 229−282. (f) Kraus, F.; Aschenbrenner, J. C.; Korber, N. *Angew. Chem., Int. Ed.* **2003**, *42*, 4030−4033.

(2) (b) Seitz, G.; Imming, P. *Chem. Rev.* **1992**, *92*, 1227−1260.

(3) Both $C_4H_4^{2+}$ and $C_4H_4^{2-}$, which are aromatic by Huckel's $4n + 2$ rule, are not a minima in D_{4h} symmetry. (a) Clark, T.; Wilhelm, T.; Schleyer, P. v. R. *Tetrahedron Lett.* **1982**, *23*, 3547−3550. (b) Hess, B. A., Jr.; Ewig, C. S.; Schaad, L, J. *J. Org. Chem.* **1985**, *50*, 5869−5871 (Correction **1986**, *51*, 4326).

(4) Maier, A.; Hofmann, M.; Pritzkow, H.; Siebert, W. *Angew. Chem., Int. Ed*. **2002**, *41*, 1529−1532. (b) Präsang, C.; Hofmann, M.; Geiseler, G.; Massa, W.; Berndt, A. *Angew. Chem., Int. Ed.* **2003**, *42*, 1049−1052. (c) Mesbah, W.; Präsang, C.; Hofmann, M.; Geiseler, G.; Massa, W.; Berndt, A. *Angew. Chem., Int. Ed.* **2003**, *42*, 1717−1719.

(5) (a) Präsang, C.; Hofmann, M.; Geiseler, G.; Massa, W.; Berndt, A. *Angew. Chem., Int. Ed.* **2002**, *41*, 1526−1529. (b) Präsang, C.; Mlodzinowska, A.; Sahin, Y.; Hofmann, M.; Geiseler, G.; Massa, W.; Berndt, A. *Angew. Chem., Int. Ed.* **2002**, *41*, 3380−3382. (c) Präsang, C.; Mlodzianowska, A.; Geiseler, G.; Massa, W.; Hofmann, M.; Berndt, A. *Pure Appl. Chem.* **2003**, *75*, 1175−1182.

(6) Pardoe, J. A. J.; Norman, N. C.; Timms, P. L.; Parsons, S.; Mackie, I.; Pulhalm, C. R.; Rankin, D. W. H. *Angew. Chem., Int. Ed*. **2003**, *42*, 571−573.

(7) (a) Albert, B. *Angew. Chem., Int. Ed.* **1998**, *37*, 1117−1118. (b) Albert, B.; Hoffmann, K. *Z. Anorg. Allg. Chem.* **1999**, *625*, 709−713.

(8) Salvador, J. R.; Bilc, D.; Mahanti, S. D.; Kanatizidis, M. G. *Angew. Chem., Int. Ed.* **2003**, *42*, 1929−1932.

(9) (a) Kaczmarczyk, A.; Dobrott, A.; Lipscomb, W. N. *Proc. Natl. Acad. Sci. U.S.A.* **1962**, *48*, 729−733. (b) Li, F.; Shelly, K.; Kane, R. R.; Knobler, C. B.; Hawthorne, M. F. *Angew. Chem., Int. Ed.* **1998**, *37*, 1868−1979. (c) Janousek, Z.; Stibr, B.; Fontaine, X. L. R.; Kennedy, J. D.; Thornton-Pett, M. *J. Chem. Soc, Dalton. Trans.* **1996**, 3813−3818. (d) Piepgrass, K. W.; Curtis, M. A.; Wang, X.; Meng, X.; Sabat, M.; Grimes, R. N. *Inorg. Chem.* **1993**, *32*, 2156−2163.

(10) (a) Wade, K. *Chem. Commun*. **1971**, 792−793. (b) Wade, K. *Adv. Inorg. Chem. Radiochem.* **1976**, *18*, 1−66.

(11) Jun, C.-S.; Powell, D. R.; Haller, K. J.; Fehlner, T. P. *Inorg. Chem.* **1993**, *32*, 5071.

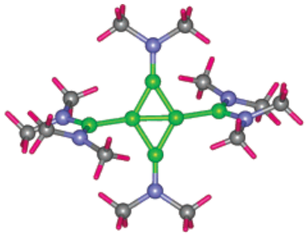

1a. $B_4(BNMe_2)_2(NMe_2)_2$
(4 bonding pairs)

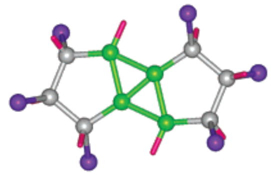

1b. $B_4H_2(C_3H_3(SiMe_3)_3)_2$
(3 bonding pairs)

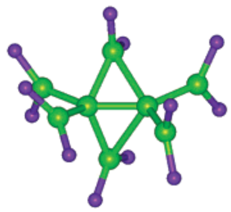

1c. $B_4(BF_2)_4F_4$
(2 bonding pairs)

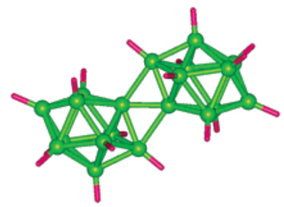

1d. $B_4H_2(B_8H_8)_2{}^{2-} \equiv B_{20}H_{18}{}^{2-}$
(no (?) bonding pairs)

Figure 1. Some discrete molecular systems containing a rhomboid B_4 skeleton. Boron atoms and boron−boron bonds are indicated in green.

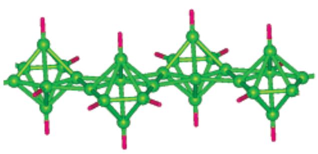

2a

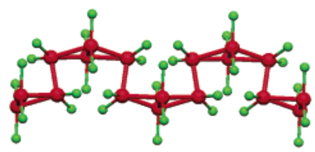

2b

Figure 2. Rhombic geometry exhibited by (a) B_4 units in Na_3B_{20} and (b) Si_4 units in β-SiB_3.

The variation in the electron counts of these simple molecular systems, sharing similar core geometry, is startling. We have not mentioned the B−B bond distances in these compounds; they are all in the range of B−B bonding, though they cover a wide span. The shortest is the B−B distance of 1.52 Å which is the central bond of the rhomboid in compound **1b**;[5] the longest 1.84 Å is in **1d**, the bond shared between the rhomboid B_4 ring and B_{10} polyhedra.[9a] We will return to the distances as we discuss the individual cases.

Extended structures add further richness. Figure 2 shows two linear chains with this rhomboid skeleton in Na_3B_{20}[7] and β-SiB_3[8] (in the latter case, the rhomboid sublattice is made out of Si rather than B). The bonding in these phases remains to be explained. Experimentally both are found to be semiconductors; calculations on β-SiB_3 show a definite band gap.[8]

For a subset of these species, **1a** and **1b**, a neat explanation of the bonding based on ideas of σ and π aromaticity is at hand.[4] In fact, some of these molecular frameworks were predicted to be stable before they were made.[12] But there is lacking a global bonding outlook that encompasses all the systems in Figures 1 and 2. This is what we seek in the present report. We begin by analyzing the bonding in the B_4 skeleton starting with a simple square B_4H_4 and from that starting point, we explore the rhomboid distortion and substitution effects systematically. From a generalized electron-counting scheme derived from this analysis, we move on to the structures of Na_3B_{20} and β-SiB_3.

(12) Neu, A.; Mennekes, T.; Englert, U.; Paetzold, P.; Hofmann, M.; Schleyer, P. v. R. *Angew. Chem., Int. Ed.* **1997**, *36*, 2117−2119.

Computational Methodology

The energies of the MOs for the molecules (as well as those of fragments) used in the interaction and correlation diagrams were derived from extended Hückel (eH) calculations.[13] Geometrical optimizations of selected molecular systems were done using the Gaussian 98 suite of programs[14] at the density functional based B3LYP/6-31G* level of theory;[15] frequency calculations characterize the nature of the stationary points. For band structures and density of states for extended structures, we employ the eH-based YAeHMOP suite of programs.[16] Further, we have also used the DFT VASP program[17] to optimize the structures and to produce the band structures for calibrating the eH results. In the VASP calculations, we chose ultrasoft pseudopotentials based on the projector-augmented-wave method[18] using the local density approximation,[19] which is ideal for arriving at equilibrium geometries. All the calculations were well converged with respect to the chosen cutoff energy and k-point sampling, unless stated otherwise.

Molecular Orbitals of Square (D_{4h}) and Rhombus (D_{2h}) B_4H_4. To understand the nature of bonding in rhomboid systems, it will be useful to analyze the evolution of molecular orbitals (MOs) with a square-rhombus distortion. The MOs of B_4 (D_{4h}) can be constructed from the valence AOs of boron, oriented conveniently into radial (p_r), tangential (p_t), and the perpendicular π sets of p orbitals (p_π), along with the s orbital set. In D_{4h} symmetry, both the s and p_r AOs transform as $a_{1g} + e_u + b_{1g}$ while p_t transform as $b_{2g} + e_u + a_{2g}$. The degenerate e_u orbitals will show the most mixing, of s, p_t, and p_r. The four MOs arising from p_π orbitals transform as $a_{2u} + e_g + b_{2u}$ and will not mix with any of the other MOs. Figure 3 shows the $B_4{}^{4-}$ (D_{4h}) MOs at left in schematic form, indicating the major contributions to the calculated MOs (at B−B 1.65 Å). Note the expected orderings: a_{2u} below e_g in the p_π set, a_{1g} below e_u below b_{1g} for the s orbitals. Some high-lying MOs are omitted.

In $B_4{}^{4-}$(D_{4h}), all four MOs that have predominant s character are filled and lie very low in energy. The all-bonding combinations of the p_π (a_{2u}), p_t (b_{2g}), and p_r (a_{1g}) are also low-lying. On interaction with four H^+ ions, as depicted in the first to second column in Figure 4 (the MOs of the four H^+ span the same irreducible representation as those of boron s and p_r), all the orbitals with substantial radial character are stabilized, as expected—their overlaps with external hydrogen atoms are largest. This is seen in the e_u, a_{1g}, and b_{1g} orbitals. In the resulting MO scheme for square B_4H_4, there are four levels very close in energy in the frontier region, with six electrons in them; this is recognizable as a typical first- or second-order Jahn−Teller situation. The distortion of a square to a rhombus will remove this approximate degeneracy.

The rhomboid distortion involves the movement of two diagonal boron atoms (B_S, S for short diagonal and L for longer diagonal) toward each other, to a bonding contact (taken as B_S−B_S 1.65 Å for the calculation shown). The molecule is still planar but the symmetry is reduced from D_{4h} to D_{2h}. The reduction in symmetry splits the

(13) Hoffmann, R. *J. Chem. Phys.* **1963**, *39*, 1397−1412.
(14) Frisch, M. J.; Trucks, G. W.; Schelegel, H. B.; Gill, P. M. W.; Johnson, B. G.; Robb, M. A.; Cheeseman, J. R.; Keith, T.; Peterson, G. A.; Montgomery, J. A.; Raghavachari, K.; Al-Laham, M. A.; Zakrzewski, V. G.; Oritz, J. V.; Foresman, J. B.; Cioslowsky, J.; Stefenov, B. B.; Nanayakkara, A.; Callacombe, M.; Peng, C. Y.; Ayala, P. Y.; Chen, W.; Wong, M. W.; Andres, J. L.; Replogle, E. S.; Gomberts, R.; Martin, R. L.; Fox, D. J.; Binkley, J. S.; Defrees, D. J.; Baker, J.; Stewart, J. P.; Head-Gordon, M.; Gonzalez, C.; Pople, J. A. *Gaussian 98*, Version 5.2; Gaussian Inc.: Pittsburgh, PA, 1995.
(15) B3LYP is Becke's three parameter hybrid method with LYP correlation functional: (a) Becke, A. D. *J. Chem. Phys.* **1993**, *98*, 5648−5652. (b) Lee, C.; Yang, W.; Parr, R. G. *Phys. Rev. B* **1988**, *37*, 785−789. (c) Vosko, S. H.; Wilk, L.; Nusair, M. *Can. J. Phys.* **1980**, *58*, 1200−1211. (d) Stephens, P. J.; Delvin, F. J.; Chabalowski, C. F.; Frisch, M. J. *J. Phys. Chem.* **1994**, *98*, 11623−11627.
(16) Landrum, G. A.; Glassy, W. V. YAeHMOP (Version 3.01) (available at http://yaehmop.sourceforge.net).
(17) (a) Kresse, G.; Hafner, J. *Phys. Rev. B* **1993**, *47*, 558−561. (b) Kresse, G.; Hafner, J. *Phys. Rev. B* **1994**, *49*, 14 251−14 269. (c) Kresse, G.; Hafner, J. *Phys. Rev. B* **1996**, *54*, 11 169−11 886.
(18) Kresse, G.; Hafner, J. *Phys. Rev. B* **1999**, *59*, 1758−1775.
(19) Perdew, J. P.; Zunger, Z. *Phys. Rev. B* **1981**, *23*, 5048−5079.

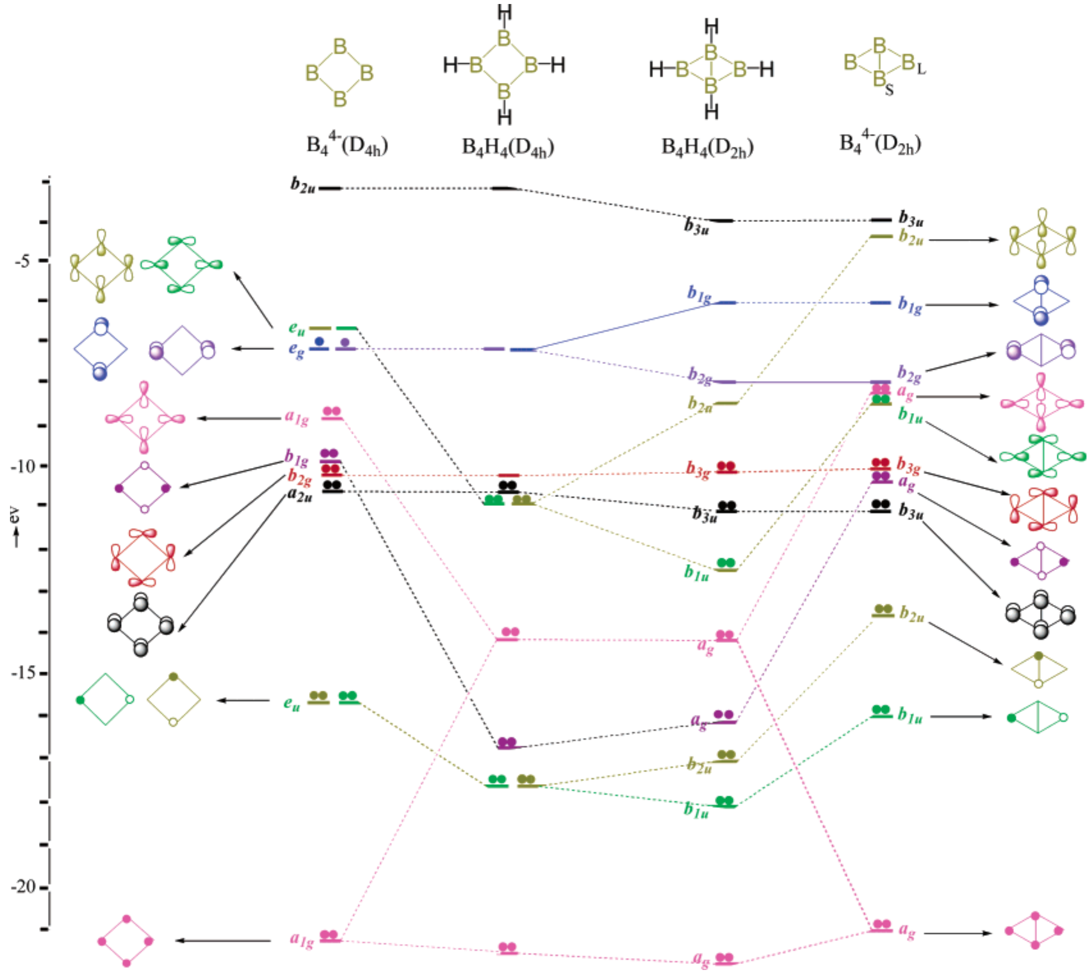

Figure 3. Correlation of MOs between D_{4h} and D_{2h} symmetry in B_4H_4 and its building blocks. MOs of differing symmetries in D_{2h} geometry are shown with distinct colors.

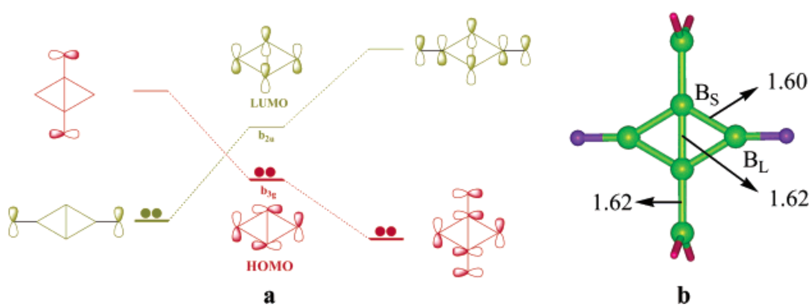

Figure 4. (a) Strategy for widening of the HOMO−LUMO gap of B_4 by the tangential π-donor and π-acceptor interactions. (b) DFT-optimized geometry of $B_4(BH_2)_2F_2$.

degeneracy of the e_u and e_g MOs. The B_4H_4 frontier e_u (which has near equal mixing of both p_t and p_r) splits strongly into $b_{2u} + b_{1u}$; the radial contribution to e_u is behind this substantial splitting. For B_4H_4 (D_{2h}), the higher member of the set (b_{2u}) is vacated, and the all-bonding tangential MO (b_{2g}) is filled. As a whole, this distortion results in a B_4H_4 framework that has a reasonable HOMO(b_{3g})−LUMO(b_{2u}) gap.

However, the gap is not large enough to ensure stability. With hydrogens as substituents, calculations indicate that neither square nor rhombus systems are minima on the potential energy surface[20] as they move toward bridging positions distorting planarity. However, the HOMO−LUMO gap can be increased (with it, likely the stability) by substitution strategies. As shown in Figure 4a, π-donors at B_L would be stabilized by the LUMO and tangential π-acceptors substituted at B_S would stabilize the HOMO. The net result of both substitutions should be a larger gap.

To substantiate this reasoning, we substituted fluorine atoms across the longer diagonal (B_L−B_L) for tangential π-donation and appropriately oriented $-BH_2$ groups (p orbital in the B_4 plane) across the shorter diagonal (B_S−B_S) as the tangential π-acceptor. The size of the substituents is kept small to allow us to explore the system at a good level of theory. The resulting D_{2h} symmetric $B_4(BH_2)_2F_2$ (Figure 4b) is a minimum on its potential energy surface at the B3LYP/6-311+G** level.

Are the deduced requirements for stabilization consistent with the molecules known in this class?[4] Reasonably so; for example, the system studied by Siebert and co-workers,[4a] $B_4(NMe_2)_2(B(NMe_2)_2)_2$ (Figure 1a), has a nearly D_{2h}-symmetric B_4 skeleton stabilized by the tangential π-acceptor $B-(NMe_2)_2$ groups across the shorter diagonal and π-donor $-NMe_2$ groups across the longer diagonal of the B_4 ring. The B_S substituents are experimentally slightly out of plane, but the external

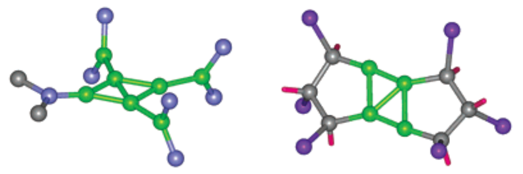

5a. $B_4(B(NMe_2)_2)_3N(Et_2)$ **5b.** $B_4(C_3H_3SiMe_3)_2$

Figure 5. Two experimentally characterized B_4R_4 molecules. The Me, Et, H, and $SiMe_3$ substituents are indicated schematically by a single "atom".

NBN groups are indeed oriented for π-acceptance (roughly perpendicular to the ring). The donor dimethylamino substituents, however, are *not* optimally oriented for π-donation, for their CNC plane is observed to be roughly in the B_4 plane. There could still be some π-type donation from C−N−C σ-orbitals. Model calculations point to a variable degree of distortion of the substituents away from the B_4 ring.[4,21,22] It may well be that steric congestion is determinative in setting the geometry and stability of this system.

Two more molecules synthesized by Berndt's group fall in this class[4b,c] (Figure 5). In molecule **5a**, the NMe_2 groups of 1a are replaced by $-NEt_2$ and $-B(NMe_2)$, groups at the longer diagonal B_L.[4b] Here, the π-donor $-B(NMe_2)$ rotates out of plane so that the NBN plane is approximately perpendicular (~81°) to the B_4 plane. In molecule **5b**, all the four substituents are replaced by alkyl groups.[4c] Calculations (not reported here) show that these substitutions increase the HOMO−LUMO gaps sufficiently so as to ensure stability.

The B_4R_4 system is very rich in its geometrical possibilities. The planar rhomboid actually occurs in a minority of the structures studied to date. B_4R_4 with R = Cl,[23] CMe_3,[24] and tmp[25] (2,2,6,6-tetramethylpiperidino) are tetrahedral. Interesting in this context is $B_4(i\text{-}Pr_2N)_4$, with a folded B_4 ring between planar and tetrahedra.[25] The rearrangement of rhomboidal B_4 to tetrahedral B_4 is symmetry forbidden, just like square-B_4 to rhomboid B_4. The later, popularly known as diamond-square-diamond rearrangement (DSD) has been repeatedly studied theoretically,[26] ever since it was first proposed by Lipscomb.[27] Braunstein et al. have studied the rearrangement of the rhomboid to a tetrahedron in transition-metal complexes.[28]

Evolution of the Skeletal MOs of the Rhomboid upon Increased *exo*-Substitution. We now move on to more complex substitution patterns. To simplify things, we leave the four most bonding MOs of B_4H_4 at the bottom (Figure 3) out of consideration. These MOs span the same irreducible representation as those subduced by four B−H bonds and we will take the lowest four orbitals primarily as such (though we are well aware that B−B and B−H bonding are mixed; more on this below). We begin then in the second column of Figure 6, and proceed to add hydrogens stepwise. D_{2h} symmetry was maintained for all of the model systems.

Consider first adding a hydrogen atom to each B_L of B_4H_4 (Figure 6) to form planar B_4H_6 (D_{2h}). In this process, two more electrons are brought to the system. The two incoming hydrogens form symmetric and antisymmetric combinations, which will interact strongly with orbitals having tangential character at B_L. One can see this in the stabilization of b_{2u} and b_{3g} as one moves from the second to the third column in Figure 6, resulting in a substantial HOMO−LUMO gap. Though B_4H_6 has two more B−H bonds than B_4H_4, only one additional MO is getting filled. Hence, we need to count b_{3g} along with b_{2u} as part of the B−H bond set, to fit a localized (2c−2e) B−H bond description. This leaves only three MOs (a_g, b_{1u}, and b_{3u}) for formal bonding in the B_4 skeleton.

Does the reduced number of framework MOs signal the weakened bonding in the rhombus? To probe this, we computed the Mulliken overlap population (OP); the results are shown in Table 1.

While moving from B_4H_4 to B_4H_6, the OP between B_S−B_L decreases, as expected. But, surprisingly, the OP increases across B_S−B_S, despite filling an additional MO (b_{2u}) which, on the face of it, is antibonding in this region. To understand this anomaly, we probed the contributions to the OP for B_S−B_S for every individual skeletal MO (Table 2).

The OP values indicate that the antibonding interaction across B_S−B_S is actually very small in b_{2u} for B_4H_6. The bonding interactions between B_S−B_S in b_{1u} and a_g are slightly increased while the

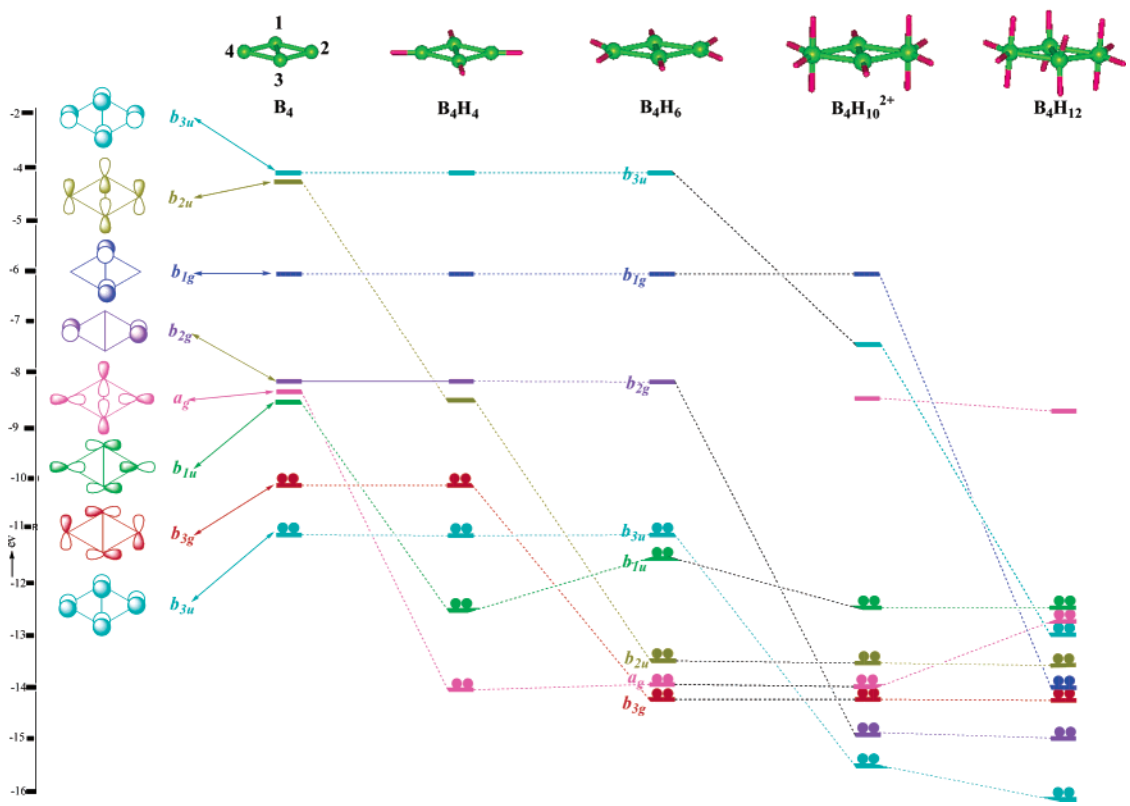

Figure 6. Correlation of the skeletal B_4 (D_{2h}) MOs with the addition of *exo* substituents. MOs of dissimilar symmetries are shown with distinct colors.

Table 1. Overlap Population between Boron Atoms in the B_4 Skeleton Obtained from eH Calculations for an Assumed Idealized Geometry (B−B = 1.65 Å, B-H = 1.2 Å)

no.	molecule	B_S–B_S	B_S–B_L	B_L–B_L
1	B_4H_4	0.514	0.820	−0.139
2	B_4H_6	0.702	0.627	−0.129
3	$B_4H_{10}^{2+}$	0.364	0.332	−0.097
4	B_4H_{12}	0.329	0.252	−0.089
5	B_4H_8	0.556	0.446	−0.134

Table 2. Overlap Population between B_S−B_S for the Skeletal MOs in B_4H_4 and B_4H_6

MO	Symm	B_4H_4	B_4H_6
	b_{3u}	0.194	0.194
	b_{1u}	0.114	0.138
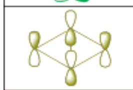	b_{2u}	-0.368*	-0.009
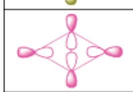	a_g	0.174	0.215
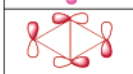	b_{3g}	-0.159	-0.011

*Not filled in B_4H_4.

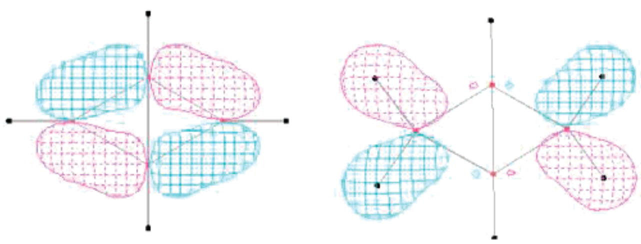

a **b**

Figure 7. b_{3g} MO of the rhombus skeleton in (a) B_4H_4 and (b) B_4H_6.

antibonding in b_{3g} is substantially decreased. Figure 7 shows the shape of the b_{3g} in B_4H_4 and B_4H_6. What a difference! The incoming hydrogens induce extensive second order mixing with high-lying b_{3g} orbitals, essentially removing the B_S contribution (and thus B_S-B_S antibonding in this MO). There is an analogous effect in the b_{2u} orbital. The system experimentally isolated by Berndt and co-workers (Figure 1b) clearly shows the B_S−B_S bond shortening implied by the OPs in Table 2—the observed B_S−B_S separation is 1.52 Å.[5]

The Limits of Assigning MOs as B−H or Framework Bonding. In the next step, we add an additional pair of hydrogens to each of the boron atoms of the longer diagonal (B_L) of B_4H_6, so that the new hydrogens lie perpendicular to the plane of the B_4H_6 ring on either side. These extra hydrogen atoms are ideally suited to interact with the perpendicular π orbitals. The resultant B_4H_{10} molecule shows a good HOMO−LUMO gap if it is a dication, as indicated in Figure 6. (Nevertheless, it is not a local minimum; appropriate substitutions may stabilize it.)

The four localized B−H bonds formed in this step would transform as $a_g + b_{2g} + b_{3u} + b_{1u}$. To find their equivalents, we have to take the stabilized b_{2g} (which was formerly empty in B_4H_6) plus the three levels that were considered framework orbitals in B_4H_6. If we assume a localized 2c−2e picture for these four B−H bonds, there remain, in principle, no electrons exclusively for skeletal bonding. But the OP value of B_S−B_S is 0.364, B_L−B_L 0.382 (see Table 1).

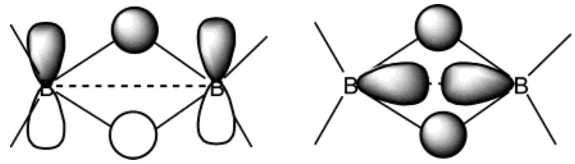

Figure 8. Two MOs of diborane which are involved in three-center B−H−B bonding.

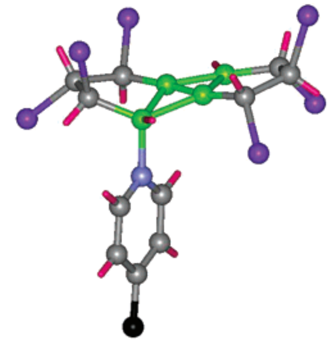

Figure 9. Structure of the experimentally observed pyridine adduct of molecule 1b.

How can there be any B−B bonding if there are no B−B bonding orbitals left? Clearly, the conceptual separation of localized B−H bonding around the rhombus B_4 ring fails at this point; a delocalized description is inevitable. An orbital-by-orbital analysis of the contributions to these overlap populations (Table 3) shows that some of the MOs which we have called B−H bonding are also B−B bonding. This is especially true for the a_g and b_{1u} orbitals. However, there is a general reduction of the overlap population values (Table 1) in the B_4 framework of $B_4H_{10}^{2+}$ compared to B_4H_6.

This situation—B−H bonding orbitals that are also B−B bonding—is to be expected. Recall the classical three-center bonding picture in diborane. The two MOs involved in the three-center bonding are shown in Figure 8. It is clearly seen that even as they are B−H−B bonding, they are also B−B bonding. In the boranes, multicenter B−B and B−H bonding separations are never clean. This is what happens in $B_4H_{10}^{2+}$, where the simple counting of framework orbitals eventually breaks down.

Base Adducts of B_4H_6. The experimentally isolated system with the B_4H_6 framework (Figure 1b) is reported to form an adduct with pyridine, at one of its B_L position, the pyridine coming in approximately perpendicular to the B_4 plane (Figure 9).[5]

Though there are four positions where one or more pyridine molecules can—in principle—attach to the B_4H_6 skeleton, only a monoadduct at B_L is reported to be formed, even when treated with excess pyridine. What happens to the MOs on stepwise addition of

(20) (a) Mach, P.; Hubac, I.; Mavridis, A. *Chem. Phys. Lett.* **1994**, *226*, 469−474. (b) Mckee, M. L. *Inorg. Chem.* **1999**, *38*, 321−330.
(21) (a) Siebert, W.; Maier, C.-J.; Maier, A.; Greiwe, P.; Bayer, M. J.; Hofmann, M.; Pritzkow, H. *Pure Appl. Chem.* **2003**, *75*, 1277−1286. (b) Sahin, Y.; Ziegler, A.; Happel, T.; Meyer, H.; Bayer, M. J.; Pritzkow, H.; Massa, W.; Hofmann, M.; Schleyer, P.v. R.; Siebert, W.; Berndt, A. *J. Organomet. Chem.* **2003**, *680*, 244−256.
(22) The bond distances of the experimental compound (B_L−B_L = 1.633, B_S−B_S = 1.605, 1.632, and B_S−B = 1.691) are comparable to our computed values for the model compound $B_4F_2(BH_2)$ (B_L−B_S = 1.60, B_S−B_S = 1.62, and B_S−B = 1.62).
(23) Atoji, M.; Lipscomb, W. N. *J. Chem. Phys.* **1953**, *21*, 172−176.
(24) Mennekes, T.; Paetzold, P.; Boese, R.; Blaser, D. *Angew. Chem., Int. Ed.* **1991**, *30*, 173−175.
(25) Maier, C.-J.; Pritzkow, H.; Siebert, W. *Angew. Chem., Int. Ed.* **1999**, *38*, 1666−1669.
(26) For example, see: (a) Mingos, D. M. P.; Johnston, R. L. *Polyhedron* **1988**, *7*, 2437−2439. (b) Wu, S. H.; Jones, M. *J. Am. Chem. Soc.* **1989**, *111*, 5373−5384. (c) Zhao, M.; Gimarc, B. M. *Polyhedron* **1995**, *14*, 1315−25.
(27) Lipscomb, W. N. *Science (Washington, DC)* **1966**, *153*, 373−378.
(28) Braunstein, P.; Debellefon, C. D.; Bouaoud, S. E.; Grandjean, D.; Halet, J.-F.; Saillard, J.-Y. *J. Am. Chem. Soc.* **1991**, *113*, 5282−5292.

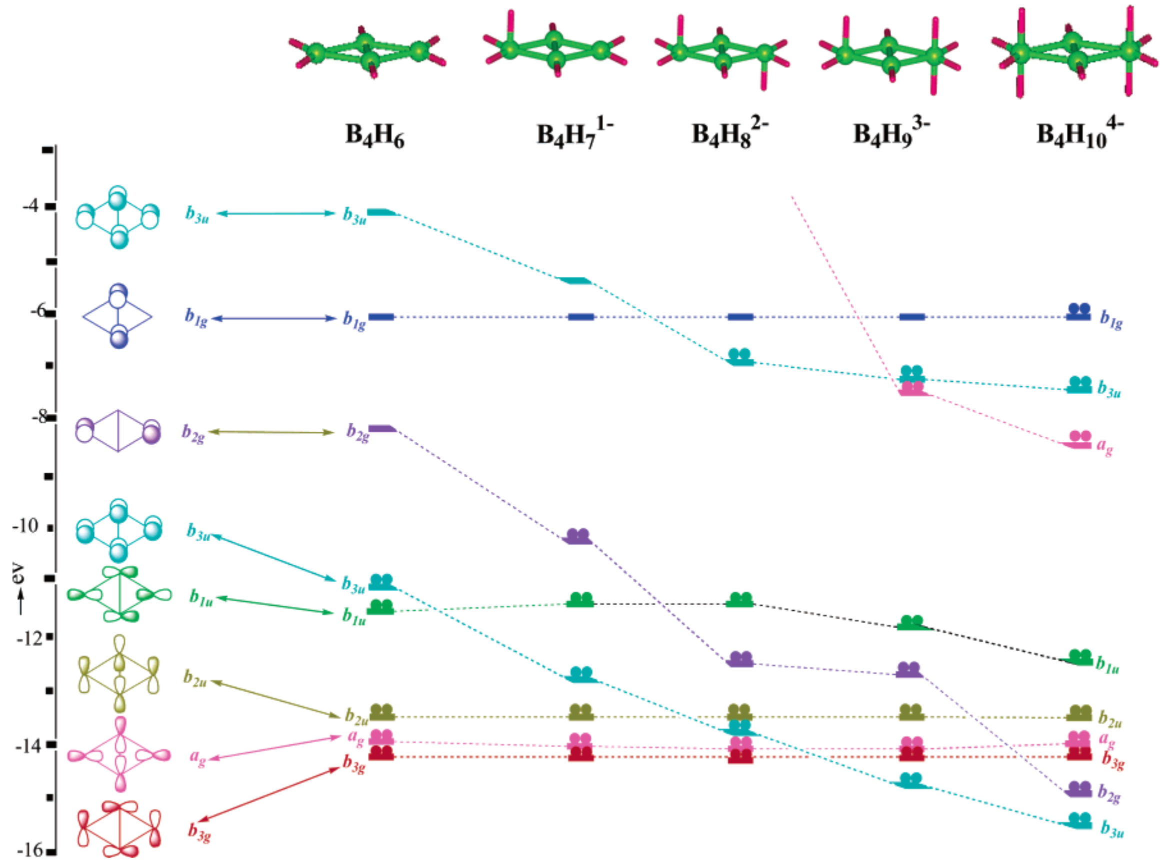

Figure 10. Correlation of the skeletal B_4 (D_{2h}) MOs due to the stepwise addition of hydride ions from B_4H_6 to $B_4H_{10}^{4-}$.

Lewis bases, here modeled by hydride ions (H^-), is illustrated in Figure 10 for addition at B_L. The full D_{2h} symmetry is lowered as one adds bases and is restored only at $B_4H_{10}^{4-}$.

The general effect is of lowering the energy of the b_{2g} and b_{3u} orbitals. But look at where the biggest electron gap is found! Adding one hydride ion (a model for pyridine) at a B_L leads to a nice gap for $B_4H_7^{1-}$ (a model for B_4H_6(pyridine)). Adding two hydrides, the gap would be large not for $B_4H_8^{2-}$, but for the neutral B_4H_8, a model for B_4H_6-(pyridine)$_2^{2+}$. The same situation prevails on the addition of three and four bases. This explains why only a single pyridine is observed to add to the compound (Figure 1b) made by Berndt and co-workers[5] (Figure 9), which is related to B_4H_6.

We also studied addition at B_S. The acceptor orbital in this case is the b_{1g}. The results are not shown in detail here, but what happens is that one H^- stabilizes the b_{1g} somewhat, so it comes a little below b_{2g}. The resulting gap is small. A second base stabilizes b_{1g} further, making a large gap for B_4H_8 neutral, which would correspond not to B_4H_6-(pyridine)$_2$ but to a dication. Perhaps this species can be made.

In the next step, we add two more hydrogen atoms to the B_4H_{10} system, to model the bonding environment of Si_4 chains in β-SiB_3 (Figure 2b). The MOs of B_4H_{12} are shown in the last column of Figure 6. Now there are four hydrogens on each side of the B_4 plane, bonded to all the four boron atoms. This results in the stabilization of all the π-MOs of the B_4 ring, of which two were initially unfilled (b_{1g} and b_{3u}). Four more electrons are required to reach a good HOMO−LUMO gap; only two come with the hydrogens, so one needs to add two more electrons ($B_4H_{10}^{2+}$ + 2H + 2e$^-$). The all-bonding radial MO (a_g) is destabilized since the hydrogens connected to boron atoms of the shorter diagonal (B_S) are moved away from the B_4 plane, but it still lies well within the bonding region.

Substitution in the B_4H_8 System. Here we consider the substituted B_4H_8 system, realized in the slightly puckered structure of $B_4(BF_2)_4F_4$ (Figure 1c). We begin by studying the nature of MO interactions between the planar B_4 ring and eight hydrogens in an idealized (D_{2h}) environment (Figure 11); the resulting B_4H_8 is a first model for B_4-$(BF_2)_4F_4$.

Since all the hydrogen atoms are positioned either above or below the plane of the B_4 ring, all the p_π MOs of the B_4 skeleton are stabilized. Even the most antibonding π MO (b_{3u}) of the ring is filled, while the all-bonding tangential MO (b_{3g}) is empty. Filling of all π orbitals essentially cancels out all the stabilization from the p_π set to the rhombus B_4 skeleton. The HOMO−LUMO gap for B_4H_8 is comparatively smaller than the gap between LUMO and LUMO + 1. The stabilization of rhomboid B_4 in this ligand environment might be achieved either by (a) stabilizing b_{3g}, and filling it by adding two more electrons or (b) raising b_{3g} in energy to increase the HOMO−LUMO gap of the neutral species. Our attempts to stabilize the all-bonding tangential MO b_{3g} with various substituents at B_L such as $-BH_2$, $-BF_2$, etc., proved futile—such substituents brought in additional levels in the frontier region, reducing the HOMO−LUMO gap. However, destabilization of the b_{3g} by π-donating substituents such as fluorine at B_L increases the HOMO−LUMO significantly, as shown in the third column of Figure 11.

DFT calculations on $B_4F_4H_4$ show two small imaginary frequencies for the D_{2h} structure; the energy minimum corresponds to a slightly puckered structure (dihedral angle 156°) with C_{2v} symmetry, about 1.2 kcal lower in energy than the planar form (Figure 12). The origin of this puckering is not clear; the energetic preference is anyway small. The long-known B_8F_{12},[29] whose structure was solved recently[6] (Figure 1c) has a similar skeleton to our model $B_4F_4H_4$ (where the hydrogen atoms are replaced by $-BF_2$ groups) but has a low symmetry (C_1) geometry, possibly due to the flat potential surface arising from the

(29) Timms, P. L. *J. Am. Chem. Soc.* **1967**, *89*, 1629−1632.

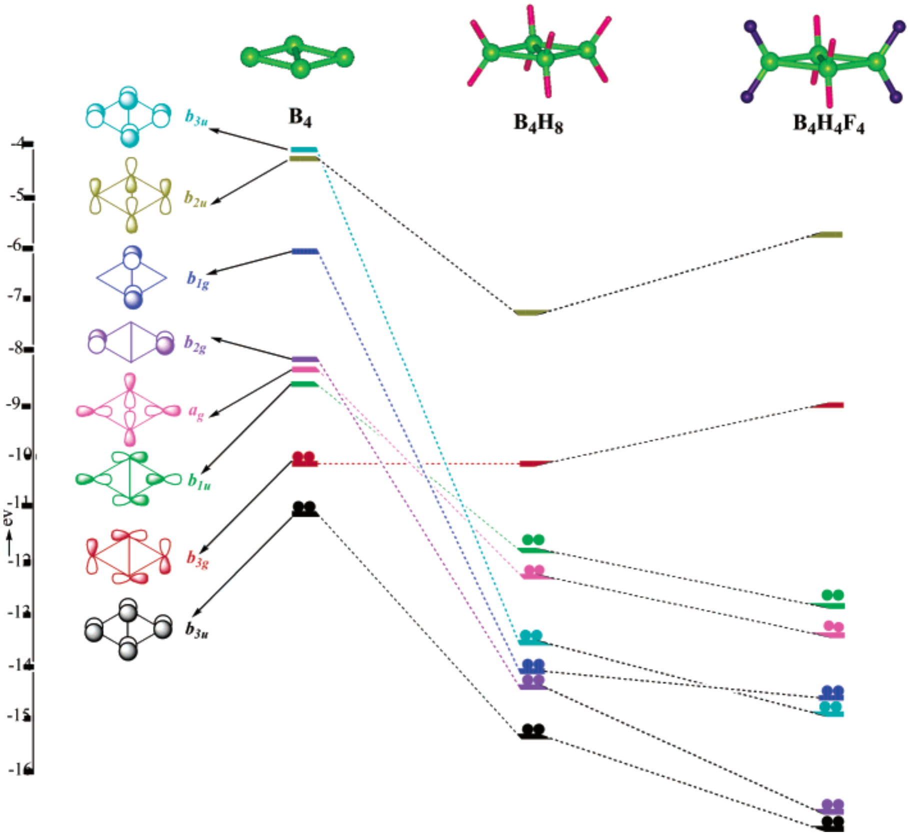

Figure 11. Interaction of MOs between the B_4 ring (D_{2h}) with eight hydrogens in the D_{2h} symmetric environment (middle). The last column shows the effect of substituting hydrogens by fluorines at B_L. MOs of dissimilar symmetries are shown in distinct colors.

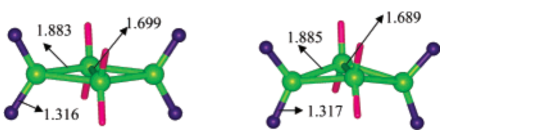

Figure 12. DFT-optimized geometries of planar (D_{2h}) and puckered (C_{2v}) $B_4H_4F_4$.

loose torsional modes of the $-BF_2$ substituents. An eH calculation on the experimentally observed geometry of B_8H_{12} gives a nice gap of 2.59 eV.

The MOs Essential for Rhomboid Bonding. The OP values within the B_4 ring decrease steadily with the addition of hydrogens, with the exception of B_4H_6 (Table 3). In our level evolution diagram (Figure 5), all these systems have four occupied MOs in common. These are the all-bonding combination of the radial (a_g), tangential p_t (b_{3g}), and π p_p (b_{3u}) and b_{1u}. The contribution of these four MOs to the net overlap population of the two B−B bonds is given in Table 4. Though we have sometimes labeled the MOs in this set as B−B bonding and sometimes as B−H bonding orbitals, it is clear from their contributions that these MOs are responsible for well over half of B_L-B_S and B_S-B_S bonding. We take this as an indication that the occupation of just these four MOs is required for a stable rhomboid ring.

A Rhomboid B_4 Unit as Part of a Macropolyhedral Borane. We now turn to the systems where a rhomboid B_4 ring fuses two polyhedral units, as in $B_{20}H_{18}^{2-}$ (Figure 1d). To count electrons in these polyhedral systems, the special electronic requirement of *rhombo*-B_4 (D_{2h}) needs to be related to the usual and successful formalism of polyhedral electron counting rules. The B_4H_4 skeleton can be reached from *closo*-$B_6H_6^{2-}$ by the removal of two capping B−H groups followed by a rhombic distortion, as shown in Figure 13, left.

From Wade's rules,[10] the electronic requirement for $B_6H_6^{2-}$ is seven skeletal electron pairs (in addition to six B−H bonds). A square planar *arachno*-$B_4H_4^{6-}$ structure is formed from $B_6H_6^{2-}$ by removing two B−H groups leaving the electrons they used in the skeletal bonding behind, i.e., $B_6H_6^{2-} \rightarrow 2(BH)^{2+} + B_4H_4^{6-}$

Table 3. Overlap Populations between Specified Atoms in the Frontier MOs of $B_4H_{10}^{2+}$

MO	Symmetry	B_S-B_S	B_S-B_L	B_S-H	B_L-H_{eq}	B_L-H_{ax}
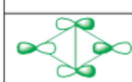	b_{1u}	0.046	0.066	0.000	0.086	0.025
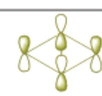	b_{2u}	-0.009	-0.028	0.103	0.154	0.000
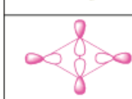	a_g	0.172	0.069	0.154	0.028	0.003
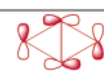	b_{3g}	-0.011	0.028	0.000	0.161	0.000
	b_{2g}	0.000	0.000	0.000	0.000	0.205
	b_{3u}	0.013	0.027	0.000	0.000	0.155

$B_4H_4^{6-}$ is also isoelectronic with cyclobutadiene dianion $C_4H_4^{2-}$ (D_{4h}). As we have seen earlier, the distortion of square $B_4H_4^{6-}$ to a rhombus leads to a good gap for a rhomboidal system (*rhombo*-B_4) with six electrons less (see Figure 3). So the *rhombo*-B_4H_4—when considered as a distorted *arachno* system derived from *closo*-$B_6H_6^{2-}$—deviates from Wade's rule by three electron pairs. We can take this as an adjustment of electron counting rules for macropolyhedral systems containing a *rhombo*-B_4 unit; we apply this "correction" in the sequel every time we encounter such a unit.

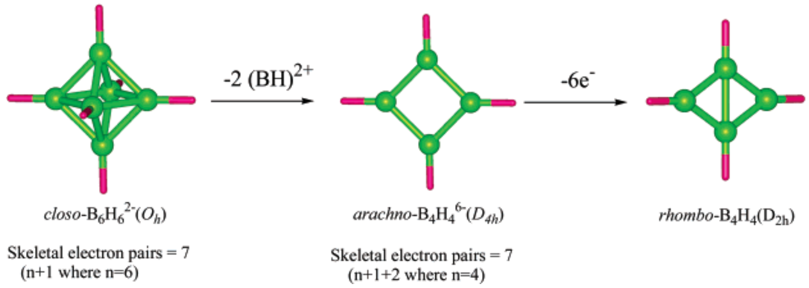

Figure 13. Schematic deduction of skeletal electron pair counting for B_4H_4 (D_{2h}).

Table 4. Contribution from the Four Skeletal MOs ($a_{1g}+ b_{3g}+ b_{3u} + b_{1u}$) to the Net B−B Overlap Populations in Different Exocyclic Environments of the B_4 Ring

	B_S–B_S overlap population		B_S–B_L overlap population	
molecule	$a_{1g} + b_{3g} + b_{3u} + b_{1u}$	net	$a_{1g} + b_{3g} + b_{3u} + b_{1u}$	net
B_4H_4	0.323	0.514	0.573	0.820
B_4H_6	0.536	0.702	0.437	0.627
$B_4H_{10}^{2+}$	0.220	0.364	0.190	0.332
B_4H_{12}	0.170	0.329	0.207	0.252

There is an alternative formulation that was suggested to us by Walter Siebert. This is to consider the *rhombo*-B_4 structural element as a "*hyper-closo*" 2n electron species instead of "distorted *arachno*". We see several problems in this formulation: (1) the term "*closo*" is traditionally understood as a skeleton that is homeomorphic to a sphere.[10] Hence, the four vertex *closo* system is tetrahedral not rhomboid. (2) The *hypo-closo*-B_4 notation will raise potential confusion with the tetrahedral B_4 skeleton that is observed in molecules such as B_4Cl_4, B_4(*t*-Bu)$_4$, etc., which are also, unfortunately, 2n electron species. For some unknown reasons, these molecules are sometimes referred to as *hyper-closo*,[30] meaning super-*closo*, even for systems such as B_8Cl_8 and B_9Cl_9, though electronically these systems are hypo rather than hyper. It is enough to make a chemist go into advertising! (3) The term "*hypo*" also has the potential to be confused with "*hypho*", which refers to the electron-rich polyhedra that have three missing vertices ($2n + 6$ species).[31] (4) *rhombo*-B_4, though experimentally known as a subsystem from the 1960s, has so far never been referred to as either *hypo* or *closo*.

To summarize, though derivation of electron count for *rhombo*-B_4 as *hypo-closo* 2n electron species looks easier, we think it is inconsistent with the definition of *closo.* And this terminology is confusing, in relation to the molecules having tetrahedral-B_4 units, which are also 2n electron species.

Nomenclature in this field clearly engenders debate. So Russell Grimes, long active in this field, in a comment on this section of the paper says, "I would question whether Wade's rule is really applicable to planar-B_4H_4, because it is not a fragment of a *closo*-polyhedron (deltahedron). In other words, when you distort square B_4H_4 to *rhombo*-B_4H_4 you are leaving Wade's country behind. In contrast, bent B_4H_4 (an octahedron minus two adjacent vertices) is a Wade structure—as in B_4H_{10} which has six additional electrons (from the six added hydrogen atoms) and in agreement with Wade's rules." We would say that *rhombo*-B_4 unit leaves Wade's country, but still prefers to live in the neighborhood.

According to a recently formulated and quite general electron-counting scheme, a macropolyhedral borane having n vertices and m cages requires $n + m$ electron pairs for optimal bonding.[32a] This scheme reduces to Wade's rule when $m = 1$, and has to be augmented with an additional "*o*" parameter which counts the number of "single-vertex sharings" in the skeleton, if available (*mno* rule).[32b] For electron counting in macropolyhedral systems containing a rhomboid B_4 skeleton, we have two options: First we may consider the *rhombo*-B_4 framework as a separate cage derived from an *arachno* skeleton; in that case, we have to subtract three electron pairs, as argued above. For example, in the case of $B_{20}H_{18}^{2-}$ (Figure 14a), the total number of vertices $n = 20$ and the number of cages $m = 3$ (including the *rhombo*-B_4 unit). The two missing capping B−H groups of the B_4 unit (making it *arachno* instead of *closo*) require the addition of two more electron pairs (see Figure 13, left). Hence by the $n + m$ rule, we need $n + m + 2$, i.e., 25 skeletal electron pairs, were the B_4 unit square planar. But, as we discussed above, the rhomboidal structural unit necessitates that we subtract three electron pairs. This results in a total of 22 electron pairs for skeletal bonding. In the molecule, there are 18 B−H group each providing one electron pair and the remaining two bare boron atoms together give three electron pairs for skeletal bonding, leading to the net −2 charge.

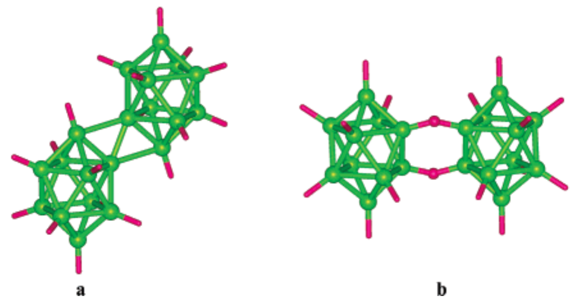

Figure 14. Structure of the $B_{20}H_{18}^{2-}$ (a) with a *rhombo*-B_4 ring flanked between two B_{10} polyhedra and (b) its photoisomer$^-$.

Alternatively, if we leave out the B_4 unit while counting the number of cages m, the total number of required electron pairs reduces to $n + m$, i.e, for $B_{20}H_{18}^{2-}$, taking $n = 20$ and $m = 2$ gives the required 22 electron pairs directly. Note that this method of electron counting formally leaves no electrons to hold the two polyhedra together in the rhombus. As we discussed above, this formal trap is a consequence of a simplistic division of framework B−B and B−H bonding. Actually, some B−H orbitals are also B−B bonding. The two approaches to electron counting are seen to be consistent. As we proceed to more complicated systems, the second method (leaving out *rhombo*-B_4 units in counting cages) has proven easier in practice. Hereafter, we leave out the *rhombo*-B_4 cages while counting m in the macropolyhedral system and apply the $n + m$ (or *mno*) rule directly.

The $B_{20}H_{18}^{2-}$ story has an interesting side to it that a reviewer has brought to our attention. This molecule is converted on photolysis to

(30) Baker, R. T. *Inorg. Chem.* **1986**, *25*, 109−111. (b) Johnston, R. L.; Mingos, D. M. P. *Inorg. Chem.* **1986**, *25*, 3321−3323. (c) Neu, A.; Mennekes, T.; Paetzold, P.; Englert, U.; Hofmann, M.; Schleyer, P. v. R. *Inorg. Chim. Acta* **1999**, *289*, 58−69. (d) Mckee, M. L.; Wang, Z. X.; Schleyer, P. v. R. *J. Am. Chem. Soc.* **2000**, *122*, 4781−4793. (e) Peynmann, P.; Knobler, C. B.; Khan, S. I.; Hawthorne, M. F. *Angew. Chem., Int. Ed.* **2001**, *40*, 1664−1667.

(31) Rudolph, R. W.; Thompson, D. A. *Inorg. Chem.* **1974**, *13*, 2779−2782.

(32) (a) Balakrishnarajan, M. M.; Jemmis, E. D. *J. Am. Chem. Soc.* **2000**, *122*, 4516−4517. (b) Jemmis, E. D.; Balakrishnarajan, M. M.; Pancharatna, P. D. *J. Am. Chem. Soc.* **2001**, *123*, 4313−4323.

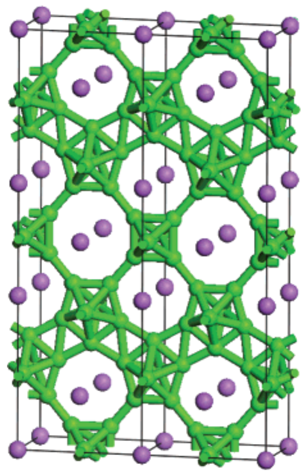

Figure 15. Structure of Na_3B_{20}.

an isomer shown in Figure 14b.[33] In this isomer, one has a "normal" structure of two B_{10} polyhedra linked by two B−H−B three-center two-electron bridges. Using this reasoning, the rhomboidal connection of the two B_{10} units in structure **14a** can also be viewed as being made up of two 3c−2e bonds. The mechanism of interconversion between these isomers is not simple, as it involves not just the movement of two hydrogen atoms to the bridging positions, but a positional shift in the boron polyhedra.

In concluding our discussion of discrete molecular systems, we should mention that we have not looked at rhomboid systems with bridging hydrogens. These deserve discussion, but even though they are common in borane chemistry in general, except for the $B_{20}H_{18}^{2-}$ isomer, they have not been seen for the rhomboid geometry.

Rhomboid Connections in Extended Systems: Na_3B_{20}. Na_3B_{20} is a recently characterized alkali metal boride,[7] found in a structural refinement of a sodium boride that was incorrectly assigned a composition of NaB_6 earlier.[34] The orthorhombic *Cmmm* structure was solved by X-ray powder diffraction and neutron diffraction. The structure has layers of alternating octahedral B_6 units and trigonal-bipyramidal B_7 units, seen from a "top" perspective in Figure 15. While the B_6 units are connected to the adjacent polyhedra by regular two center bonds, the adjacent B_7 units are fused by the now familiar *rhombo*-B_4 unit, similar to the fusion of the B_{10} units in the molecular $B_{20}H_{18}^{2-}$. In forming infinite chains of B_7/B_4 units, the topological arrangement is such that the adjacent B_4 units share a unique single vertex. Na_3B_{20} is reported to be an insulator.[7b]

The orthorhombic unit cell of Na_3B_{20} ($Z = 2$) can be conceptually divided into $(Na)_6(B_6)_2(B_7)_4$ units for the purpose of electron counting. While the two electron requirement of B_6 can be directly deduced from Wade's rule, the B_7 units which are fused by *rhombo*-B_4 units require the application of the mno rule. Each B_7 chain has two B_7 and two B_4 units in the unit cell. Hence $n = 14$, $m = 2$, and $o = 2$, which gives a total of 18 electron pairs per chain or an anticipated count of nine electron pairs per B_7 unit. For every repeat unit of the B_7 chain, there are four boron atoms with *exo*-2c−2e bonds connecting the other polyhedra. These boron atoms formally contribute one electron pair each to skeletal electron count. The remaining three boron atoms of the B_7 unit have no *exo*-2c−2e bonds, and they together contribute 4.5 electron pairs (3×3 valence electrons) to skeletal bonding. We thus have a situation where a B_7 unit has 17 electrons (8.5 electron pairs) but by the *mno* rule requires 18 electrons for stability. The B_7 unit should then acquire an extra electron from the rest of the lattice for stability, as B_7^{1-}. The charge assignment of individual units in Na_3B_{20} that polyhedral electron counting then leads us to is $(Na^+)_6$ $(B_6^{2-})_2$ $(B_7^{1-})_4$, which gives—by this electron-counting scheme—a net −2 charge per unit cell or −1 charge per formula unit. We would conclude from this formalism that Na_3B_{20} (neutral) is electron deficient, not optimally bonded.

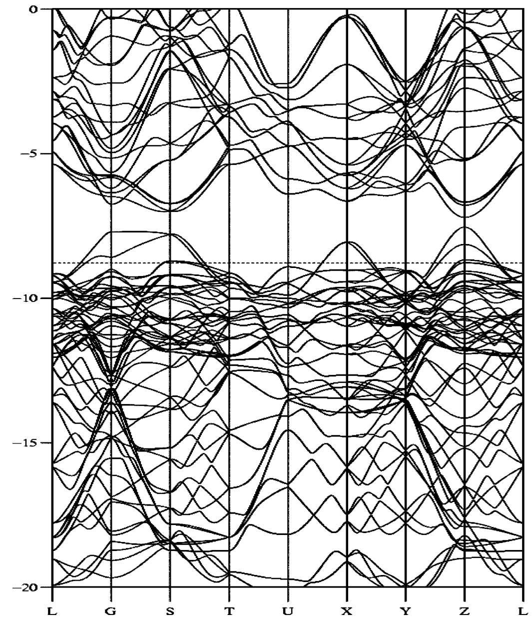

Figure 16. Band structure of Na_3B_{20} from eH calculations.

To verify this additional requirement for electrons, extended Hückel calculations including the Na atoms were carried out for the orthorhombic cell of Na_3B_{20}, where $Z = 2$. The band structure calculation indicates metallic behavior for the neutral species but shows a finite band gap for a −2 charge, confirming our electron-counting ideas (Figure 16). Contributions to the projected density of states of boron atoms in the B_6 and B_7 polyhedra (Figure 17a,b) show that bands crossing at the Fermi level of the neutral species are predominantly from the B_7 polyhedra.

To confirm the validity of *mno* rule for this unprecedented single vertex sharing of B_4 units, we performed molecular DFT calculations on some discrete molecular borane chains containing two, three, and four B_7 units (Figure 18). For the dimer, $n = 14$ and $m = 2$, thus requiring 16 electron pairs by the $n + m$ rule. The 12 B−H groups provide 12 electron pairs and two shared boron atoms give three electron pairs, resulting in a total of 15 electron pairs. So this molecule needs two more electrons to satisfy the $n + m$ rule, just like the molecular $B_{20}H_{18}^{2-}$ discussed above.

Geometry optimization followed by frequency calculations at the B3LYP/6-31G* level of theory shows that the dimer $B_{14}H_{12}^{2-}$ is a minimum on the potential energy surface with a 2− charge and reasonable B−B distances. A neutral $B_{14}H_{12}$ moves away from the idealized geometry. For the trimer, $n = 21$, $m = 3$, and $o = 1$, so by the *mno* rule, the molecule requires 25 electron pairs for skeletal bonding. The 16 B−H groups and five shared boron atoms together contribute only 23.5 electron pairs, three electrons short of the *mno* rule count. Similar counting gives a 4− charge for the tetramer ($n = 28$, $m = 4$, $o = 2$). All these molecules are minima with respective charges calculated by the *mno* rule, at the same level of theory.

EH band calculations on infinite one-dimensional chains of B_7H_4 (Figure 2a) show a band gap (Figure 19) of about 2 eV when provided with a −1 charge per B_7 unit, as expected from the argument above. Here, the B−B distances are kept at 1.75 Å and B−H distances are kept at 1.2 Å, typical bond distances observed for polyhedral boranes. The topmost band of the 1D-chain is quite steep, starting at −8.6 eV at Γ and descending to −10 eV at X, spanning a bandwidth of around

(33) (a) Hawthorne, M. F.; Pilling, R. L. *J. Am. Chem. Soc.* **1966**, *88*, 3873−3874. (b) DeBoer, B. G.; Zalkin A.; Templeton, D. H. *Inorg. Chem.* **1968**, *7*, 1085−1090.
(34) Hagenmuller, R.; Naslain, R. *C. R. Acad. Sci.* **1963**, *257*, 1294−1296.

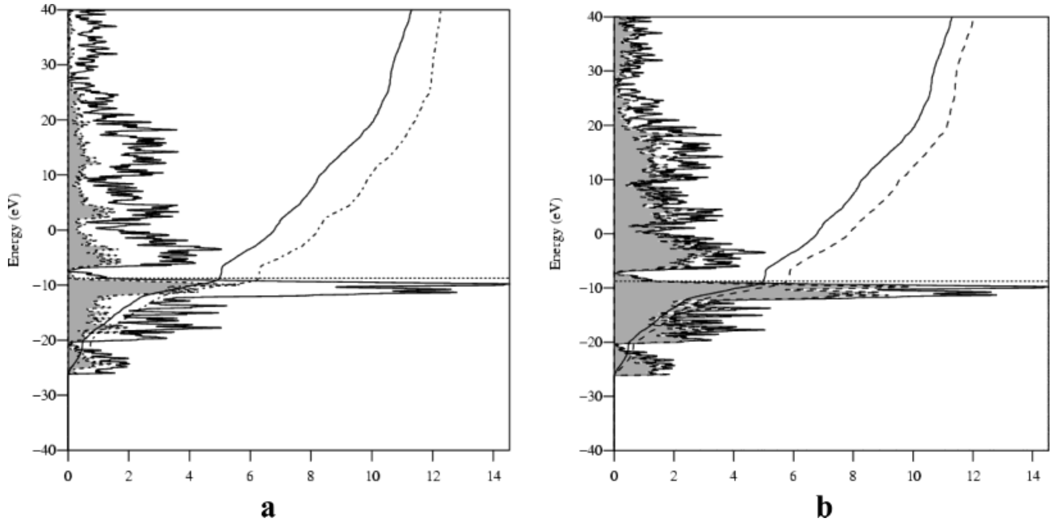

Figure 17. Projected density of states for the atoms of (a) B_6 and (b) B_7 polyhedra in Na_3B_{20}.

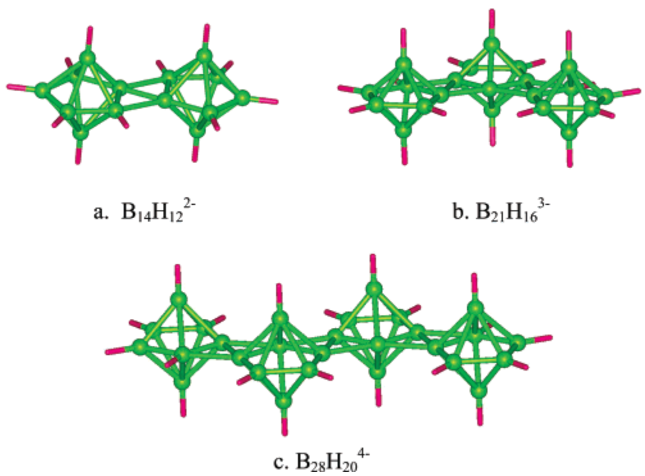

Figure 18. Optimized structures of discrete molecules having B_7 polyhedra linked with rhombic B_4 units at the B3LYP/6-31G* level of theory.

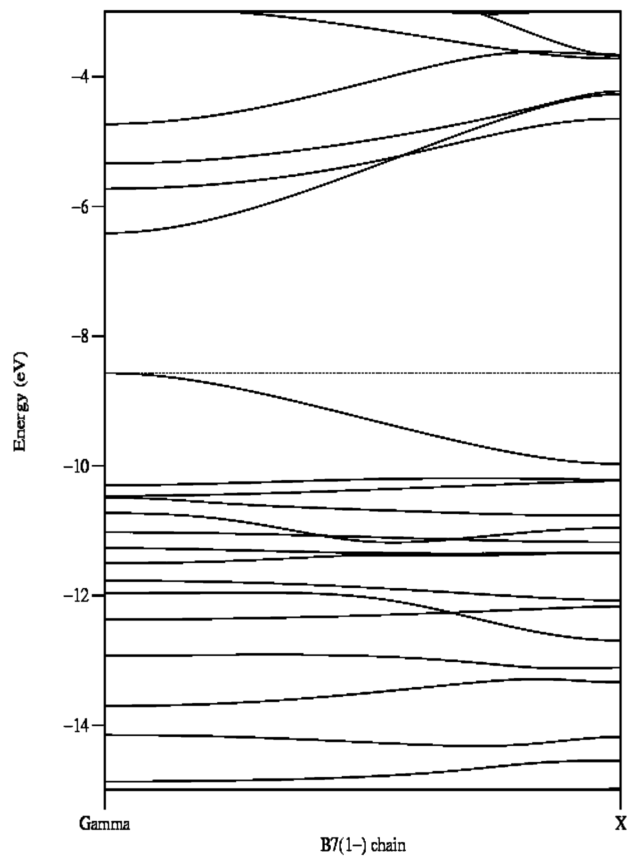

Figure 19. Band structure of one-dimensional chain of $(B_7H_4^{-1})_n$.

1.4 eV. This indicates substantial inter-unit cell interaction in the frontier MOs of this polymer.

Returning to Na_3B_{20}, we studied the electron deficiency of the neutral structure with DFT calculations, optimizing the primitive unit cell (Z = 1) with +1, 0, and −1 charges. We used a plane-wave cutoff energy of 400 eV with a k-point separation of about 0.04 Å^{-1} (9 × 9 × 12 mesh). Our repeated attempts to obtain the converged geometry for neutral and +1 charged unit cell by using increased cutoff energy, and k-point sampling proved futile. However, the system with a −1 charge converged rapidly. The optimized primitive unit cell of $Na_3B_{20}^{-1}$ ($a = b$ = 9.771 Å, c = 4.090 Å; $a = b$ = 90.0°, γ = 146.43°; cell volume = 215.919 Å^3) is in reasonable agreement with the experimentally reported unit cell parameters ($a = b$ = 9.757 Å, c = 4.14 Å, $\alpha = \beta$ = 90.0°, γ = 146.09°, cell volume = 220.347 Å^3) from neutron diffraction. The band structure of Na_3B_{20} obtained from eH calculations using the DFT-optimized geometry is given along with the DFT bands in Figure 20. The band structures appear similar, except that the band gap of ~1 eV obtained from eH calculations vanishes in the DFT band structure, which shows a zero band gap, near special point Y (−0.5, 0.5, 0) in the Brillouin zone.

We have a problem: (1) electron counting and our calculations point to Na_3B_{20} needing more electrons, and (2) it is hard to see how Na_3B_{20} with an odd number of electrons in a primitive unit cell (as found) can be insulating. Insulating behavior due to localization of states (a Mott transition) seems to be improbable, due to the steep nature of the bands from B_7 chains in the frontier region. One can think of two possible mechanisms by which the system can get its extra electrons: (a) partial occupancies or (b) interstitial atoms. Sodium vacancies, i.e., partial occupancy of sodium sites, moves the electron count in the wrong direction. Even partial occupancy of boron sites in this system will increase the electron deficiency, as it will give rise to partially open "*nido*" structures, which demand more electrons. The possibility of having interstitial Na^+ ions is also unlikely, due to the compact packing. The heptagonal channels in the boride network already contain sodium atoms with nearest Na−Na contacts ~4.14 Å.

We suggest that there are in this structure some interstitial boron atoms, capping the faces of the polyhedra. Such capping boron atoms are known to provide additional electrons to the framework without modifying the electron count, in structures such as β-rhombohedral

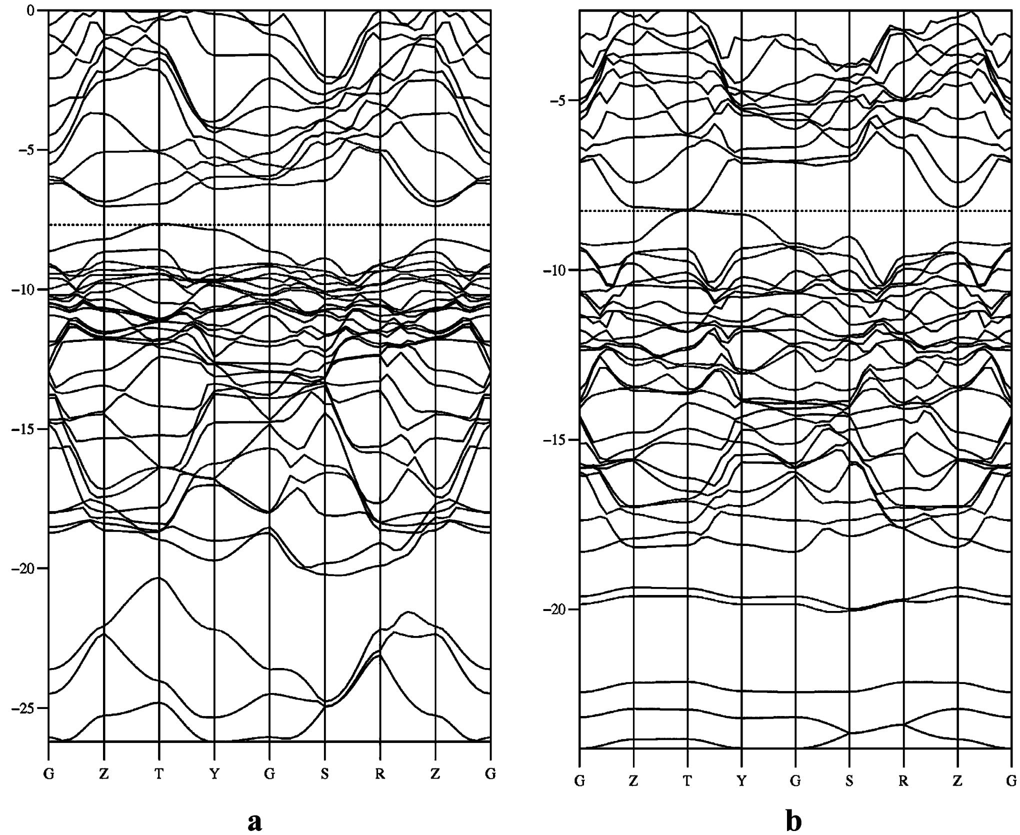

Figure 20. Band structure of the optimized $Na_3B_{20}^{-1}$ from (a) eH and (b) DFT calculations.

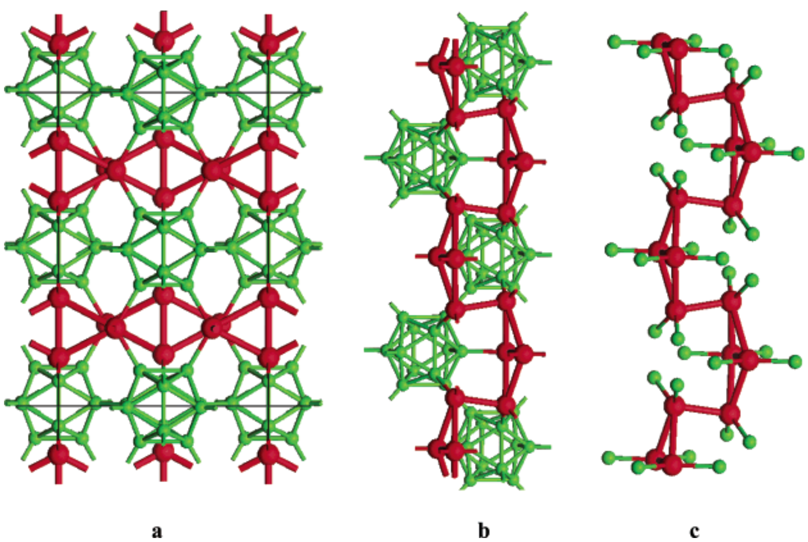

Figure 21. Structure of β-SiB_3: (a) unit cell, (b) alternative view showing Si_4 chains, (c) coordination environment of Si_4 chains.

boron. The mechanism has been described by Mingos et al. as the "capping principle".[35] Since there are many three-membered ring faces available in the unit cell, the capping atoms may be randomly distributed in different faces. This would make their experimental detection by diffraction methods difficult. In summary, further structural investigation of this phase is indicated; the electronics argue strongly against a simple Na_3B_{20} stoichiometry.

A reviewer has suggested that there might be a carbon substituting the boron leading to the composition $Na_3B_{19}C$. However, the analytical data in the original work[7b] seems to exclude the presence of any other atom other than boron and sodium.

(35) Mingos, D. M. P.; Welch, A. J. *J. Chem. Soc., Dalton Trans*. **1980**, 1674−1681.

A Silicon Realization of the Rhomboid Framework in β-SiB_3. The electron-deficient rhomboid skeleton is not restricted to boron. Silicon, which is diagonally related to boron, also exhibits this unit in the recently reported β-SiB_3 structure.[8] Among the known binary phases of silicon and boron, β-SiB_3 (space group *Imma*) is the only phase that is crystallographically well-ordered without any partial occupancies or vacancies. It was well characterized using single-crystal X-ray diffraction studies. Two views of the β-SiB_3 structure, along with the extracted coordination environment of the Si_4 chains in the structure are given in Figure 21.

The structure of β-SiB_3 consists of layers of B_{12} units linked together, and a layer of interconnected rhombic Si_4 units forming sinuous chains as shown in Figure 21. These infinite Si_4 chains connect to the remaining

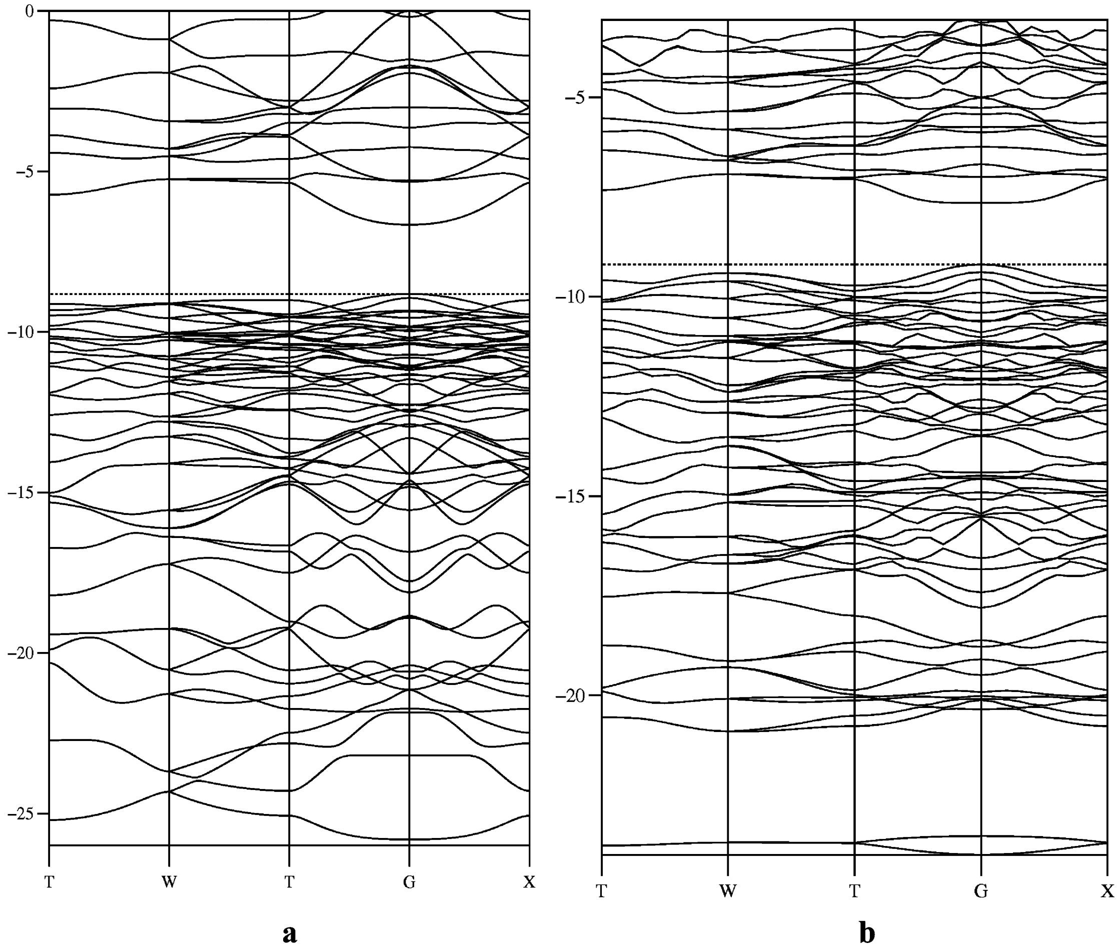

Figure 22. Band structure of β-SiB$_3$ from (a) extended Hückel and (b) DFT calculations.

dangling bonds of the B_{12} polyhedra. Both experimental measurements and DFT band structure calculations characterize the compound as a semiconductor with a definite band-gap.[8] The bonding in β-SiB$_3$ remains unexplored. The band structure obtained from eH calculation for β-SiB$_3$ is given in Figure 22a.

For calibrating the parameters employed in eH calculations, we also performed a DFT optimization of SiB_3 using a plane wave cutoff energy of 400 eV with a $5 \times 5 \times 5$ k-point set. The band structure obtained from DFT calculations is given alongside the eH bands as Figure 21b. There is a direct band-gap of ~1.5 eV observed in both calculations, in good agreement with the earlier reports.

For the purpose of electron counting, we divide the orthorhombic unit cell of β-SiB$_3$ ($Z = 16$) into $(B_{12})_4(Si_4)_4$. Since each B_{12} unit requires two electrons, the Si_4 unit has to be assigned a +2 charge.[8] We can relate the environment of the Si_4 units to the neutral rhomboidal B_4H_{12} model discussed earlier. Each Si_4 unit differs somewhat from B_4H_{12}, as two of the four axial hydrogen atoms are missing on one side. So the appropriate model will be the doubly deprotonated $B_4H_{10}^{2-}$, which is isoelectronic to $Si_4H_{10}^{2+}$. To confirm the electronic requirement, we carried out DFT calculations on the discrete $Si_4H_{10}^{2-}$ molecule with a C_{2v} symmetric constraint. Frequency calculations indicate that $Si_4H_{10}^{2+}$ (C_{2v}) is not a minimum on its potential energy surface; the axial hydrogens at the longer diagonal are trying to move toward the bridging positions, breaking the symmetry. The replacement of axial hydrogens with $-SiH_3$ groups will simulate an ideal model for the environment around Si_4 units in β-SiB$_3$, but the loose torsional modes of $-SiH_3$ in practice will complicate the computations, due to the flat potential energy surface they engender. Hence, we decided to replace the two axial hydrogens with fluorine atoms. The resulting $Si_4H_8F_2^{2+}$ (Figure 23) is a minimum. The bond length variation is more pronounced in

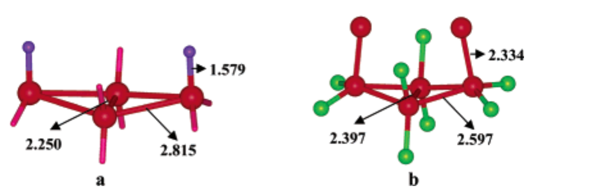

Figure 23. The geometry of (a) optimized $Si_4H_8F_2^{2+}$ and (b) $(Si_4^{2+})_n$ unit in β-SiB$_3$.

$Si_4H_8F_2^{2+}$ compared to the observed distances in β-SiB$_3$, presumably due to the higher electronegativity of fluorine.

Since the eH method gives a band structure very similar to that of the quantitatively more accurate DFT calculations on β-SiB$_3$, it is easy to test the effect of chain formation in Si_4 units on its charge. Figure 24 shows the band structure and density of states for the one-dimensional Si_4H_8 polymer with a 2+ charge per unit cell. There is a substantial band gap (~5 eV), confirming that the linking of Si_4^{2+} units does not alter the charge requirements.

The bonding in β-SiB$_3$ thus can be conveniently interpreted as built up from B_{12}^{2-} polyhedra and novel nonclassical Si_4^{2+} units, analogous to boron rhomboids.

Conclusion

The electronic requirements of systems exhibiting the rhomboid geometry, quite diverse, are explained using molecular orbital theory. There are four MOs which are primarily responsible for skeletal bonding. A bridge is built between molecular *rhombo*-B$_4$ systems and polyhedral extended structures with an analogous building block. We think the recently

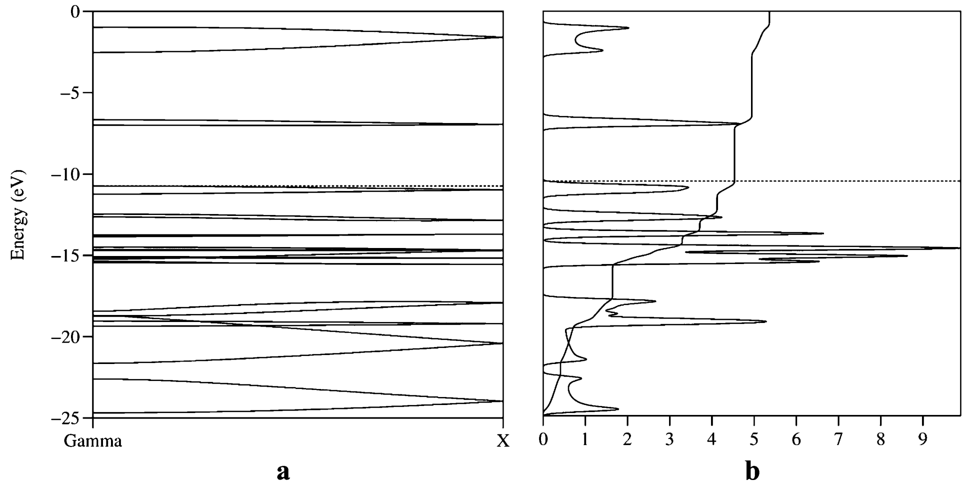

Figure 24. (a) Band structure and (b) density of states of 1-D $Si_4H_8^{2+}$ chains.

reported structure of Na_3B_{20} (which contains the *rhombo*-B_4 units) is electron deficient and requires one more electron per formula unit to explain the observed insulating behavior; we suggest there may be interstitial boron atoms in this structure. We have also related the bonding in β-SiB_3, which contains rhomboid Si_4 units, to that of molecular and extended *rhombo*-B_4 structures.

Acknowledgment. Our work was generously supported by the National Science Foundation through research grant CHE-0204841. We are grateful to Armin Berndt, Russell Grimes, Walter Siebert, and the reviewers for their comments on our paper.

Supporting Information Available: Cartesian coordinates for relevant molecules optimized at B3LYP/6-31G* level and fractional coordinates for relevant extended structures optimized with DFT based LDA/PAW calculations. This material is available free of charge via the Internet at http://pubs.acs.org.

JA0467420